Article

Experimental and Numerical Analysis of Wooden Sonic Crystals Applied as Noise Barriers

Tommaso D'Orazio [1], Francesco Asdrubali [2], Luís Godinho [3,*], Matheus Veloso [3] and Paulo Amado-Mendes [3,*]

[1] Department of Philosophy, Communication and Performing Arts, Roma Tre University, Via Ostiense 139, 00154 Roma, Italy; tommaso.dorazio@uniroma3.it
[2] Department of Industrial, Electronic and Mechanical Engineering, Roma Tre University, Via Vito Volterra 62, 00146 Roma, Italy; francesco.asdrubali@uniroma3.it
[3] ISISE, ARISE, Department of Civil Engineering, University of Coimbra, R. Luis Reis dos Santos 290, 3030-790 Coimbra, Portugal; matheusdveloso190689@gmail.com
* Correspondence: lgodinho@dec.uc.pt (L.G.); pamendes@dec.uc.pt (P.A.-M.)

Abstract: Recent research has been developed by different groups towards the development of sonic crystals as noise barriers. The present paper aims to contribute to this research, focusing on the possible application of this technology in practice, and exploring some aspects that may be useful for its further development. One of the objectives of this work is to explore the differences between experimental results obtained under laboratory conditions and numerical results computed with the finite element method (FEM), in 2D and 3D, understanding if different types of simplified models can be of use in the practical analysis of sonic crystals. Through this comparison, a validation of the prediction numerical models is performed, giving confidence for their use in the development and study of sonic crystal configurations. In this context, different geometric arrangements of the sonic crystals' scatterers (the individual elements that make up the barriers) have been analyzed with the help of the numerical method, evaluating their behavior in different arrangements of numbers of elements, shape and size. A number of parametric studies are also performed introducing some randomness in the structure (in scatterer size and spacing), and analyzing its effect on the insertion loss provided by the sonic crystal. These contributions can be significantly useful for the development of new solutions, giving important hints about the sensitivity of these structures to possible defects or limitations in their production.

Keywords: noise barriers; sonic crystals; periodic structures; insertion loss; band gap; wooden barriers; experimental analysis; finite element method

1. Introduction

The continuous growth of vehicular traffic and the large number of exposed people have made sleep disturbance and the annoyance caused by road traffic noise important problems encountered by citizens [1]. Several studies have shown that exposure to road traffic noise can induce additional adverse health effects, including cardiovascular effects [2], learning disabilities [3] and ischemic heart disease hypertension [4]. Damage due to long lasting exposure to noise can directly affect the hearing organ and can be assessed in terms of temporary, or permanent, hearing loss or speech perception difficulties. There are also other damages due to continuous exposure to noise that affect the human body in a wider way, producing an increase in blood pressure, chronic stress syndrome, mental disorders, psychosomatic symptoms or behavioral disorders. In addition, noise affects the performance, quality and duration of sleep in various ways [5], and the awareness of the negative effects that noise can have on the health or well-being of the individual causes a general feeling of annoyance, that can be expressed in a sense of discomfort and a feeling of discontent.

Exposure to road traffic noise can be reduced by applying mitigation strategies near the sources, such as improving engine protection and vehicle design [6] or reducing noise emissions due to tire/road contact with special surfaces or with policies directed towards reducing vehicle travel needs. However, these actions are not always convenient or adequate, or can even be almost ineffective, and therefore the implementation of noise barriers represents the most common solution to further reduce people's exposure to traffic noise.

The presence of an obstacle, such as a noise barrier, between the noise source (the vehicles) and the receiver, affects the propagation of the acoustic waves and effectively attenuates the disturbing noise levels. In general, in the interaction with an obstacle's surface, the sound waves are partly reflected, partly absorbed and partly transmitted. Conventional noise barriers combine sound-absorbing and sound-insulating elements; that is, they attenuate road traffic noise by absorbing and reflecting the incident sound energy and reducing the sound transmission through the obstacle. For this purpose, conventional barriers are made of compact and dense materials, so that the sound energy transmitted through the barrier can be considered limited. From the spectral point of view, traditional barriers have good insulation behavior over the entire traffic emission spectrum, generally between 100 Hz and 5 kHz, but mainly from 500 Hz to 1500 Hz [7].

However, conventional noise barriers present several drawbacks, such as diffraction phenomena at the edges which significantly reduce noise attenuation. In fact, due to diffraction, sound waves propagate over the top or lateral extremities of an obstacle, reducing the noise-shadowing effect behind the barrier [8]. In addition, traditional noise barriers without any surface absorbent treatment can reflect the sound energy back across the roadway towards the receivers on the opposite side [9], and they can present problems related to the size of the structure, since a compact noise barrier of variable length and height represents a strong environmental impact by limiting people's field of view and reducing natural light [10].

In order to minimize the aforementioned disadvantages, in recent years, research has focused on the study of noise barriers based on sonic crystals. These are artificial periodic structures that are not homogeneous, formed by discrete elements (scatterers) spatially arranged in a periodic configuration with a square, triangular or rectangular lattice and that exhibit a high contrast of properties to the acoustic medium in which they are embedded (i.e., the air) [11]. Due to its periodic nature, this arrangement of scatterers exhibits a band gap at a well-defined frequency range, at which noticeable sound attenuation occurs. It should be noted that, in contrast with traditional barriers, the diffraction effect is expected to be less pronounced due to the irregular nature of the borders (top or lateral), which are made of several isolated objects instead of a continuous edge; in addition, the discontinuous character of the barrier generates a strong dispersion of the incident energy, avoiding specular reflections even when rigid scatterers are used.

Among the advantages associated with the use of this technology, it is also important to note the low weight and ventilation capability of the structures. In fact, the openness of these barriers allows a limitation on the loads acting on the foundation and a reduction in their costs [12], decreasing the overturning moment due to wind or shock wave from high-speed vehicles. This type of "more open" noise barrier also allows some continuity of the visibility and passage of air through the discrete elements forming a lower visual impact barrier [13] and contributing to higher social acceptance.

In the present paper, a contribution to the state of the art of sonic crystal barriers is given, presenting data values observed from experimental tests and comparing them to numerical results computed through finite element method (FEM) models. Simulations were also performed for different scatterer arrangements and shapes, analyzing noise barriers' behavior, the attained insertion loss values and the computed dispersion curve diagrams. Of particular relevance to the topic is the comparison between 2D, 3D and experimental results, since the importance of height in sonic crystal structures and the associated diffraction effect occurring on the top of the barriers is significantly different from that of traditional barriers. In addition, the effect of possible changes in the periodic

arrangement due, for example, to production issues is also evaluated, discussed and quantified, an aspect that is quite relevant for the future production of technical solutions of this type.

2. Noise Barriers Based on Sonic Crystal Concepts

Periodic structures are composed of a regular and repetitive geometric arrangement of elements. Their macroscopic characteristics are greatly dependent on the manufacturing geometry and, in general, they can significantly modify the propagation behavior of the waves passing through them.

The first studies in this research topic were undertaken in 1887, by Rayleigh [14], and the first realization of these concepts was proposed by Veselago [15], in 1968, for the propagation of electromagnetic waves. Later, other studies were developed by Yablonovitch [16] and John [17], focusing on photonic crystals in metals and semiconductors, since the atoms that make up these elements are arranged in a periodic lattice and photonic band gaps are formed. The wave propagation behavior in periodic structures is described by Bloch's theorem [18], which has been derived for electromagnetic waves in perfect crystals. The solution of the Bloch wave for a periodic potential leads to the formation of bands of allowed and forbidden energy regions, i.e., the band gaps. The same principle can be extended and applied to sound waves as they propagate through periodic structures. When the acoustic waves interact with periodic structures, bands of frequencies are formed, where waves can pass through the structure without too much attenuation, while in other ranges of frequencies waves are greatly reduced. This leads to a significant attenuation of sound levels in selected frequency bands.

The first experimental measurements of sound attenuation by a sonic crystal structure were reported by Martinez-Sala, in 1995 [19]. This study is based on the analysis of Eusebio Sempere's artistic sculpture, composed of a periodic arrangement of stainless-steel tubes, installed in the gardens of the Fundación Juan March, in Madrid. The structure was based on a minimalist design and consisted of hollow steel rods, with a 3 cm outside diameter, arranged in a square lattice with a constant distance between the centers of the rods of 10 cm. This pioneering work experimentally demonstrated, for the first time, the filtering capabilities of sound in a real periodic structure. These authors have shown that the periodic arrangement of steel tubes causes multiple interferences (constructive and destructive) between the acoustic waves. This behavior has been identified as frequency-dependent behavior, since the transmitted waves are attenuated at certain frequencies, while it has little or no effect on other parts of the spectrum. Subsequently, in other studies, the researchers highlighted the effect on noise attenuation of this type of periodic structure, with different configurations of geometries and materials, finally creating real sonic crystals. Sigalas and Economou [20], for example, achieved good levels of acoustic attenuation and were able to observe a band gap by performing the same experiment on the sculpture using the plane wave expansion method.

The physical mechanism that governs this phenomenon observed in periodic structures is Bragg's law, derived following experiments on electromagnetic waves, in 1913 [21]. It states that the destructive interference of a wave hitting the crystal lattice with an angle of incidence, θ (see Figure 1), determines a band gap influenced by the density ratio, M, between the density of the material of the scatterers and that of the medium in which they are immersed (air), leading to a central frequency of the band gap, expressed as follows:

$$f_{BG} = \frac{c}{2\alpha\,sin\theta},\qquad(1)$$

being dependent on the lattice constant, α, i.e., the distance between two adjacent scatterers, and on c, the sound propagation speed in the medium (in air, $\simeq$343 m/s) [22]. In fact, Bragg's law essentially expresses the condition for the interference between the diffracting waves from the various crystalline planes to be destructive.
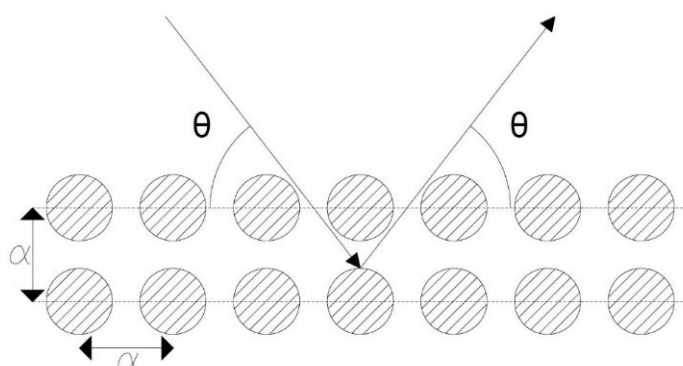
Figure 1. Schematic illustration of Bragg's law with an incident wave at angle θ on a crystal periodic structure with lattice constant α.

To calculate the sound level reduction provided by periodic structures, the concept of insertion loss (*IL*) can be introduced, which describes the loss of power of the acoustic signal at a certain point due to the insertion of the barrier.

The insertion loss is expressed as:

$$IL = 20 \, \log_{10} \frac{P_T}{P_R},\tag{2}$$

where P_T is the sound pressure registered before the barrier is introduced and P_R is the observed sound pressure, at the same point, after the introduction of the barrier. The sound attenuation provided by the acoustic barrier, calculated in dB, is therefore evaluated as the difference between the average sound pressure levels measured with and without the sonic crystal barrier.

The physical and geometric arrangement of the entire sonic crystal can be defined by specifying the content of a single unit cell, whose periodic repetition generates the crystalline structure. Therefore, each unit cell is characterized by a lattice constant, *α*, and a filling fraction, *ff*. The lattice constant is a parameter relating to the physical and geometric size of the unit cell and quantifies the distance between centers of neighboring scatterers, while the filling fraction is the ratio between the volume occupied by the single scatterer and the volume of the entire elementary cell [21].

Band gap phenomena occur when the sonic crystal exhibits a certain filling fraction. If the filling fraction is small, the propagation of the wave inside the crystal is not affected by the presence of scatterers and the dispersion relationship assumes linear values [23]. For periodic structures to interact with waves, the size of the scatterers and the spacing between them must be of the order of the wavelength of the propagating wave; for example, the wavelength of sound waves, in the audible region (20–20 kHz), ranges from approximately 17 mm to 17 m [21].

The main target application of the type of noise barrier under study is traffic noise mitigation, which is known to have particular relevance around the frequency of 1000 Hz. Indeed, international standards such as the ISO 717-1 [24] or EN 1793-3 [25] present the reference noise spectrum shown in Figure 2, where it is clear that the most relevant sound pressure levels occur between 630 Hz and 2000 Hz.

In the literature, some experimental studies have already been presented in previous works and, in fact, Iannace et al. [26] tested noise barriers consisting of small-scale (1:10) wooden scatterers. Santos et al. [27] and Amado-Mendes et al. [28] tested reduced-scale sonic crystal barriers consisting of PVC scatterers, while Morandi et al. [23,29] carried out laboratory tests on full-scale PVC barriers. Furthermore, other studies have analyzed sonic crystal barriers with different cross-sectional geometries of scatterers. Pichard et al. [30] and Cavalieri et al. [31] studied sonic crystals consisting of square cross-section scatterers, while Rubio et al. [32] studied scatterers with a rectangular section and Alagoz et al. [33] studied triangular cross-section scatterers. Koussa et al. [34] studied the effects of a sonic crystal coupled with a traditional barrier. On the other hand, Cavalieri et al. [31] studied

the mitigation of sound by sonic crystal barriers applied to the noise produced by trains, and Koussa et al. [35] analyzed the mitigation of sound due to low-height sonic crystal barriers applied to the noise produced by trams, while Lee et al. [36] considered a children's maze made up of sonic crystals. Furthermore, sonic crystals can also consist of the periodic arrangement of trees; Gulia and Gupta [37] achieved a reduction in noise impact by modeling rows of Thuja trees arranged in a periodic pattern on the sides of a road. A significant attenuation of the sound, with a maximum of 19 dB, was obtained in frequencies up to 500 Hz, consistent with what was reported by Martínez-Sala et al. [38], demonstrating that properly arranged trees can be used to mitigate noise pollution while helping to reduce air pollution and vibrations to the receivers. Numerical approaches have instead been used and can herein be referred to, namely the method of fundamental solutions (MFS) used by Godinho et al. [39] while studying infinite 3D sonic crystals, or the boundary element method (BEM), adopted by Jean and Defrance [40] in the analysis of sound propagation through infinite rows of cylindrical elements along roads.
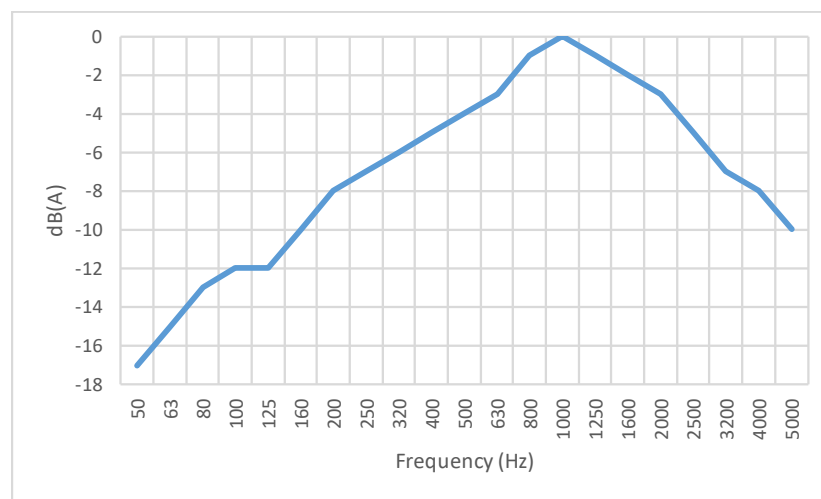
Figure 2. Road traffic noise spectrum, adapted from ISO 717-1, and normalized to a maximum of 0 dB(A).

The concept studied in this work corresponds to a highly sustainable solution, with the structural elements being made up of wood logs obtained from forest thinning operations. The use of small-diameter wood logs in structural applications, such as roofs, building frames and bridges has already been studied around the world. In particular, in Portugal, extensive research work has been carried out in the characterization of round timber logs obtained from forest thinning operations of maritime pine (*Pinus pinaster*) [41]. This species is the main variety of conifers in Portugal, with an abundant number of trees harvested from thinning operations throughout the country. In addition to the environmental use of this type of timber, it also satisfies the main requirements for the elements that form the wooden sonic crystal barrier, such as the dimensions and the mechanical properties. Furthermore, in terms of sustainability, the expected efforts and loads acting on the periodic wooden structure only require the low processing of the timber logs, such as a lathe and conservative treatment, thus minimizing costs and environmental impact. After evaluating the mechanical behavior of the structural elements, their mechanical properties were found to be similar or often superior to those obtained for wood available from other species, and significantly superior to those of other more processed wood elements such as scatterers with a rectangular cross-section [13].

In the following sections of the present work, the study of the acoustic attenuation of road traffic noise levels making use of sonic crystals noise barriers is proposed. This analysis has been carried out by developing experimental tests in the laboratory using sonic crystal barriers with cylindrical scatterers made of 1:3 scale pine wood logs. The results thus obtained from the laboratory experiments have been compared with numerically

computed values resulting from the simulations performed through the finite element method (FEM) and its implementation within the Matlab software.

3. Materials and Methods

3.1. Laboratory Work

In order to experimentally test the behavior of acoustic barriers formed by sonic crystals, a set of measurements was performed at the acoustics laboratory of the Department of Civil Engineering of the University of Coimbra (DEC-UC). The semi-anechoic chamber existing in the laboratory was treated with a layer polyurethane foam, also simulating a highly absorbing floor and resulting in an anechoic environment. Using this experimental setup, it became possible to avoid significant reflections from the walls and the floor, that would disturb the measurement results.

The sonic crystal barriers that were tested in the laboratory present two types of geometric arrangements, namely barriers with scatterer distributions in rectangular and in triangular spatial lattices. In both types of arrangements, the scatterers, which are made of pinewood circular logs with a diameter of 4 cm, were arranged in four rows. Figure 3 schematically illustrates the arrangements, for which a lattice constant of α = 6 cm has been adopted.

(a)　　　　　　　　　　　　　　　　　　　　　(b)
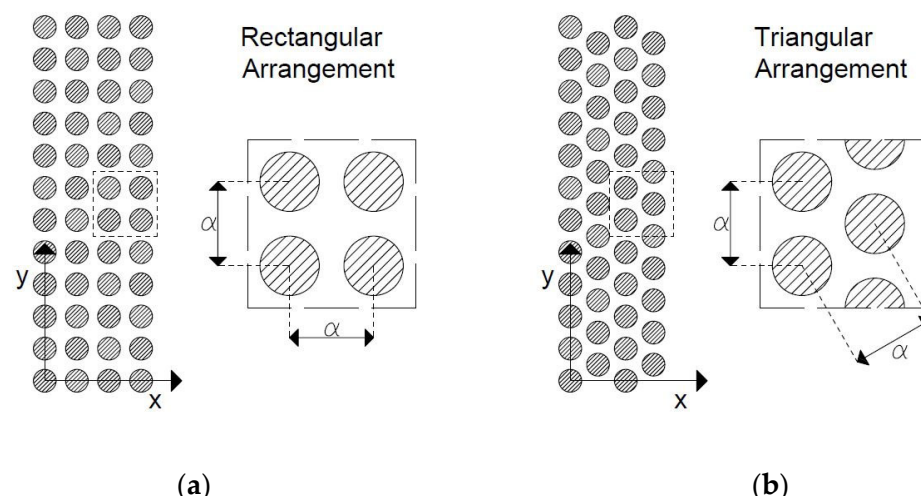
Figure 3. Different geometric arrangements of the sonic crystal barriers, in plane view: (**a**) rectangular lattice arrangement; (**b**) triangular lattice arrangement.

The barrier prototypes tested in the laboratory present filling fraction (*ff*) values of 0.35 (for the rectangular arrangement) and 0.40 (for the triangular arrangement). These experimental prototypes can be seen, in fact, as a smaller-scale reproduction of a sonic crystal barrier concept made of pine wood logs, under development in the University of Coimbra; on a real scale, these would correspond to circular scatterers with a diameter of 12 cm, and a lattice constant of 18 cm. The sonic crystals barriers built in the laboratory correspond to models faithful to real noise barriers, but manufactured on an approximate reduced scale of 1:3, while maintaining the same filling fraction as that of the full-scale barriers. Two different heights have been adopted for the prototype noise barriers used in the experimental tests, namely 1.2 m high and 0.6 m high, corresponding to sonic crystal noise barriers 1.80 m and 3.60 m tall in a real setting. Figure 4 presents two pictures of specimens with these two heights, after being mounted in the anechoic room in the laboratory.

The sound source used in the laboratory tests consists of a loudspeaker, positioned at a distance of 35 cm from the barrier, centered with its height, and two sets of four receivers were defined for evaluation of sound pressure levels (SPL), with the microphones placed on the opposite side of the noise barrier. The first set of four microphones was placed 10 cm behind the barrier while the second set was placed 30 cm from the barrier; the

height of the microphones was defined so that two of them were 15 cm below the center of the source, and the other two were placed 15 cm above it. Furthermore, in the direction parallel to the barrier, two of the microphones were placed at a distance of 20 cm to the right of the sound source axis and the other two were placed 20 cm to the left of the sound source axis. Average SPLs were evaluated using the eight measurement positions, and considering the scenarios with and without the sonic crystal barrier. Using the described setup, the insertion loss of the reduced-scale barriers was then calculated as the difference between both scenarios. In Figure 5, a schematic illustration of the experimental setup can be observed, through the lateral and plane layouts of the laboratorial tests for the case of the barriers that were 1.20 m tall.


(**a**)

(**b**)
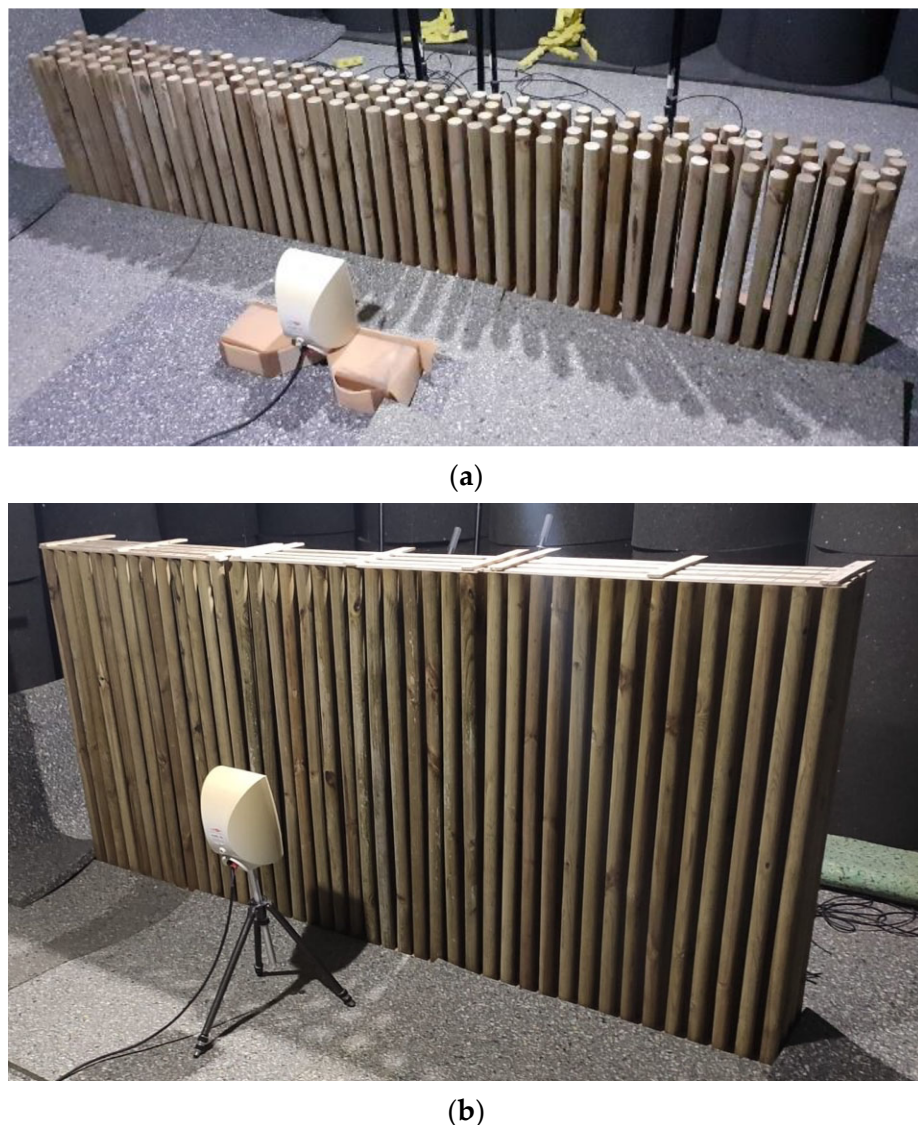
Figure 4. Small-scale sonic crystal noise barrier prototypes, made of wood logs, mounted in the acoustics laboratory of the DEC-UC: (**a**) barrier 0.6 m tall; (**b**) barrier 1.2 m tall.

The SPL measurements were performed making use of a National Instruments NI-USB 4431 acquisition system, with four 1/2″ microphones and pre-amplifiers from GRAS Sound & Vibration, models 40AF and 26AK; in these tests, a broadband-spectrum white noise signal was used, emitted through an Alpha 100 RTO loudspeaker.

(a)¤　　　　　　　　　　　　　　　　　　　　　　**(b)**¤
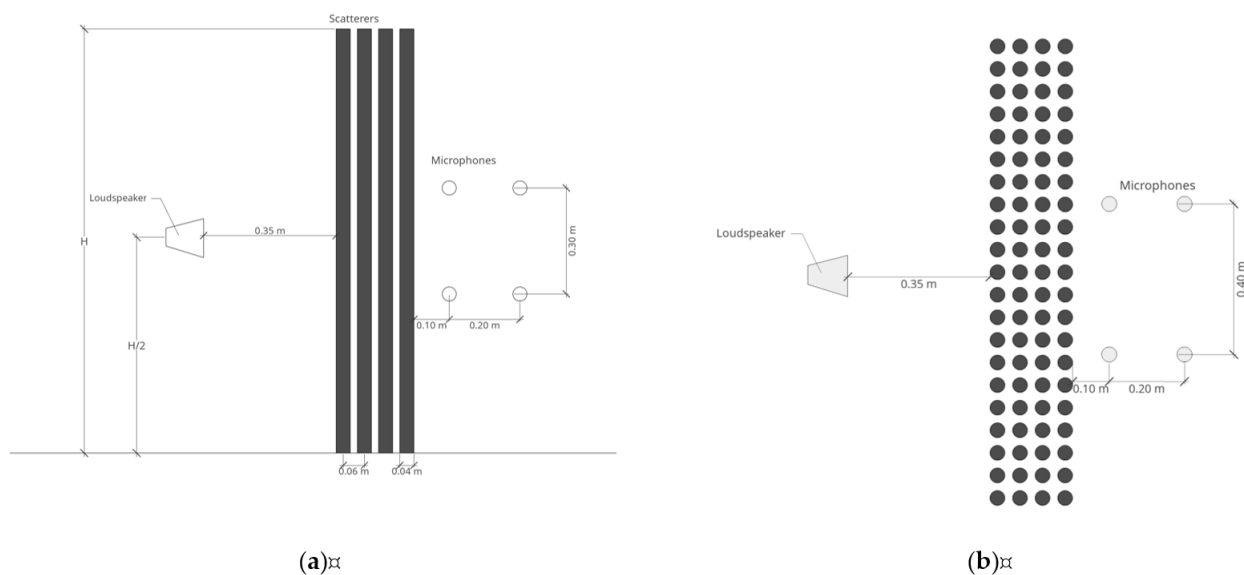
Figure 5. Schematic representation of the experimental setup for the case of 1.2 m tall sonic crystal noise barriers: (**a**) lateral view; (**b**) plane view.

3.2. Numerical Simulations

Numerical simulations were performed using the finite element method (FEM), formulated in the frequency domain, allowing us to obtain approximate, but accurate, solutions for the governing Helmholtz equation:

$$\nabla^2 p + \frac{\omega^2}{c^2} p = 0, \tag{3}$$

with ω being the angular frequency, c being the sound propagation velocity and p being the acoustic pressure. Since the application of the FEM for the engineering analysis of complex problems is now widely accepted, and a wide bibliography is available regarding this numerical method, only a very general FEM overview is here presented, and the reader is referred to well-accepted references, such as [42] for further details. The frequency domain FEM formulation used here is based on the classical equation

$$\left(K + i\omega C - \omega^2 M \right) p = f(\omega), \tag{4}$$

where K is the stiffness matrix, $i = \sqrt{-1}$ is the imaginary number, C is the damping matrix, M is the mass matrix, p is the nodal sound pressure vector and $f(\omega)$ is the vector of the external applied forces. Two types of models have been used in the present work, namely a 3D and a 2D discretized model, in both cases only accounting for the fluid (acoustic) domain. The first was used mainly for comparison with experimental results obtained in the laboratory, allowing us to account for the finite height and length of the acoustic barrier, while the second type of model was used both for that purpose and to perform a set of parametric analyses.

The simulations performed with the FEM models concerned the two types of scatterers' geometrical arrangements, described before, namely with rectangular and triangular lattice distributions. In all cases, periodicity was considered along the longitudinal direction (y axis in Figure 5b). Below, some details of the 3D and 2D models are given.

3.2.1. 3D FEM Models

Acoustic problems require special care in mesh definition, since the accuracy strongly depends on the mesh element size and on the analyzed phenomena's wavelength. For the present case, and to ensure accurate numerical results, in the 3D implemented models, 8 node tetrahedra elements were adopted, with quadratic shape functions, always ensuring

a minimum of 5 elements per wavelength for the most unfavorable discretization. Since these models were used to simulate the experimental (laboratory) setup conditions, with periodicity along the longitudinal *y* direction, a strip with half the size of the lattice constant was modeled in 3D, and a numerical perfect matched layer (PML) was introduced at the top and lateral boundaries of the discretized models, thus avoiding spurious reflections into the simulation domain. For the floor, a simplified impedance condition was used to simulate the absorbing nature of the laboratory floor materials, thus ascribing a condition of the type $Z = \rho c$. The numerical 3D FEM models were created in order to reproduce the exact size of the laboratory setup (reduced-scale sonic crystal noise barriers), and a range of frequencies between 300 Hz and 4800 Hz has been calculated. A line load, positioned 35 cm from the barrier and centered with the barrier's height, has been defined as the emitting source. The number of finite elements required for these models ranged from approximately 152,000 to 366,000, while the number of nodes varied from 243,000 to 578,000, depending on the height of the barrier modeled. Figure 6 presents a generic schematic representation of the 3D numerical model implemented and of the adopted FEM mesh.
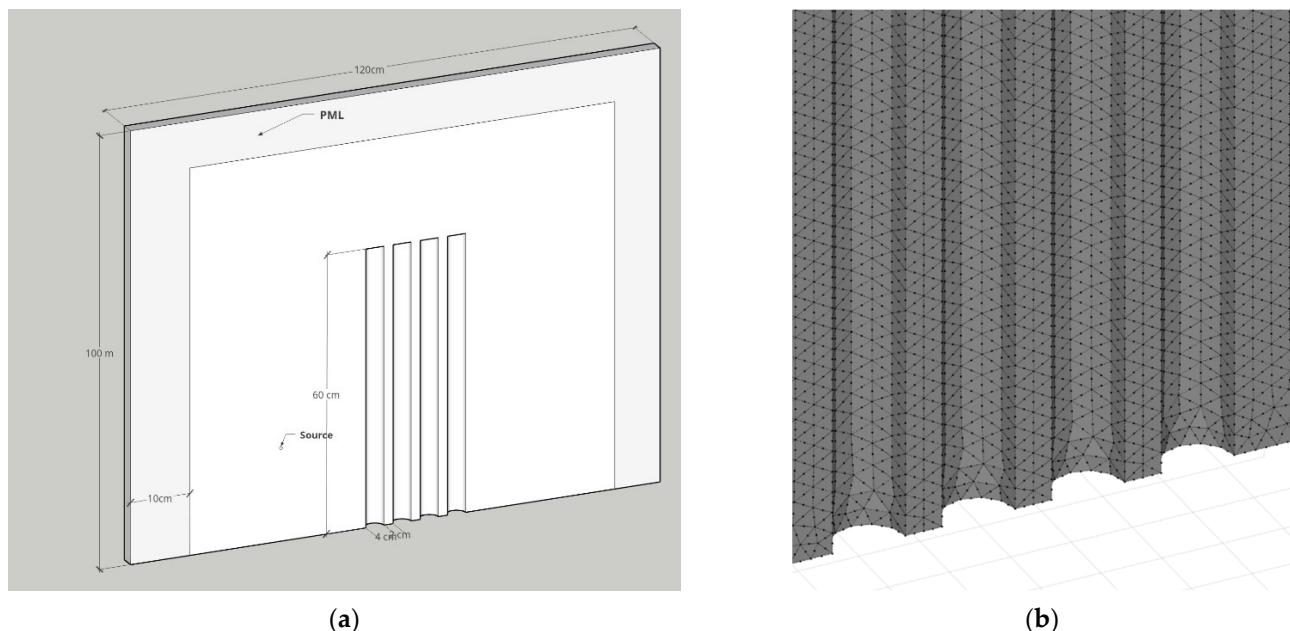

Figure 6. 3D numerical model: (**a**) schematic representation of a 60 cm tall sonic crystal barrier; and (**b**) detail of the 3D FEM mesh around sonic crystal elements of the barrier with four lines of scatterers.

3.2.2. 2D FEM Models

For the 2D numerical models, 3 node triangular elements were used in the spatial discretization of the domain; since these are much simpler finite elements and since the computational cost of the 2D problems is substantially lower, a maximum length of the element side of 1/9 of the acoustic wavelength was adopted, in order to allow for a good level of accuracy. To ensure a more accurate discretization of the circular geometry of the scatterers, a more refined mesh has been defined around the sonic crystal elements. Then, around 10,000 elements were used for each case modeled.

As already stated, in order to minimize computational cost, only a part of the problem was considered in the modeling process, assuming periodicity along the longitudinal direction of the crystal sonic noise barrier, thus allowing us to discretize just a strip of the complete barrier and physical domain, as illustrated in Figure 7. In that figure, examples of the finite element mesh, generated for the rectangular and triangular lattices, can be observed. The red lines represent the boundaries of the problem modeled, where the following boundary conditions are imposed: in the shorter sides (top and bottom), absorbing boundary conditions were imposed, corresponding to an air impedance of $Z = \rho c$; for the

scatterers, rigid wall conditions were imposed, corresponding to null particle normal velocity; on the left and right (longer) boundaries, periodic boundary conditions were prescribed, which for the present case, in which normal incidence plane waves are considered and the geometry is symmetric, correspond to just imposing null particle velocity conditions at those boundaries; finally, to simulate the generation of a plane wave, a unit load per meter was considered at the bottom boundary.

(**a**)   (**b**)
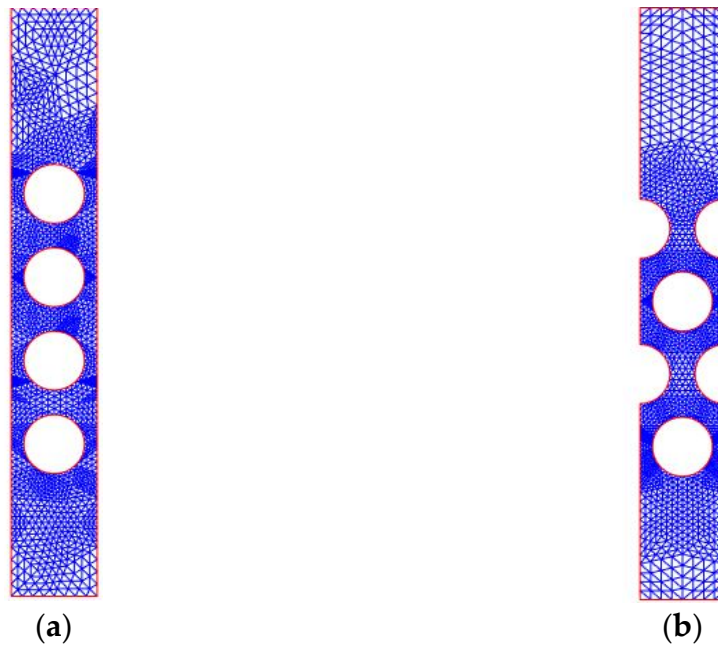
Figure 7. Discretization mesh of 2D FEM models: (**a**) rectangular, and (**b**) triangular geometric arrangements of sonic crystal elements.

4. Results and Discussion

4.1. Small-Scale Experimental and Numerical Results

The first set of results presented in this work corresponds to a validation of the numerical approaches proposed here for the simulation of the sonic crystal noise barriers. For that purpose, the experimental setup described in a previous section was used, considering four different reduced-scale scenarios:

- A barrier 1.2 m tall, with a rectangular arrangement of the scatterers;
- A barrier 0.6 m tall, with a rectangular arrangement of the scatterers;
- A barrier 1.2 m tall, with a triangular arrangement of the scatterers;
- A barrier 0.6 m tall, with a triangular arrangement of the scatterers.

These laboratory prototypes are, as referred to, scaled-down representations of a real scale noise barrier (approximately at a geometric scale of 1:3), and were built using four rows of wooden circular poles, thus replicating the expected behavior of the real sustainable noise barrier. The IL acoustic performance provided by each of these prototypes was measured following the described procedure, and the experimental data were processed and compared with those of 2D FEM and 3D FEM models, both assuming that the crystal sonic noise barrier represents an infinitely long and periodic structure. Results from the experimental measurement and numerical modeling simulations are depicted in Figure 8, for the four reduced-scale cases. One should note that the frequency range indicated in the plots (300 Hz to 4800 Hz) corresponds to the real measurement range registered in the laboratory. Although the three approaches for evaluation of the IL have some fundamental differences (in terms of source type and 2D or 3D character), this comparison can be useful precisely to have a clearer view of what the differences are between the different models, and what the error committed is when the problem is simplified to 2D representation.

By comparing the experimental results with those derived from the numerical calculations, for the rectangular geometric distribution of the scatterers of the barriers, it can be observed that the trend of the acoustic attenuation values provided by the noise barriers is similar, although with some differences in the amplitude. Although the 3D simulations seem to better reproduce the experiments, outside the band gap the approximation provided by both FEM models is quite similar. For both numerical and experimental approaches, the IL values show low acoustic attenuation for the lower frequencies up to about 1600 Hz and reveal a rising band gap ranging from about 1600 Hz to 3700 Hz. In the numerical approach, moreover, it can be noted that the most attenuated frequency also coincides with the central frequency of the band gap which is around 2800 Hz (considering the lattice constant of 6 cm). From the results of the experimental work, on the other hand, the central frequency remains around the same frequency, but with a lower peak of IL attenuation. It is interesting to note that the difference between the smaller and taller barriers is not very significant, both exhibiting quite similar behavior and IL values, both in the 3D model and in the laboratory measurements.
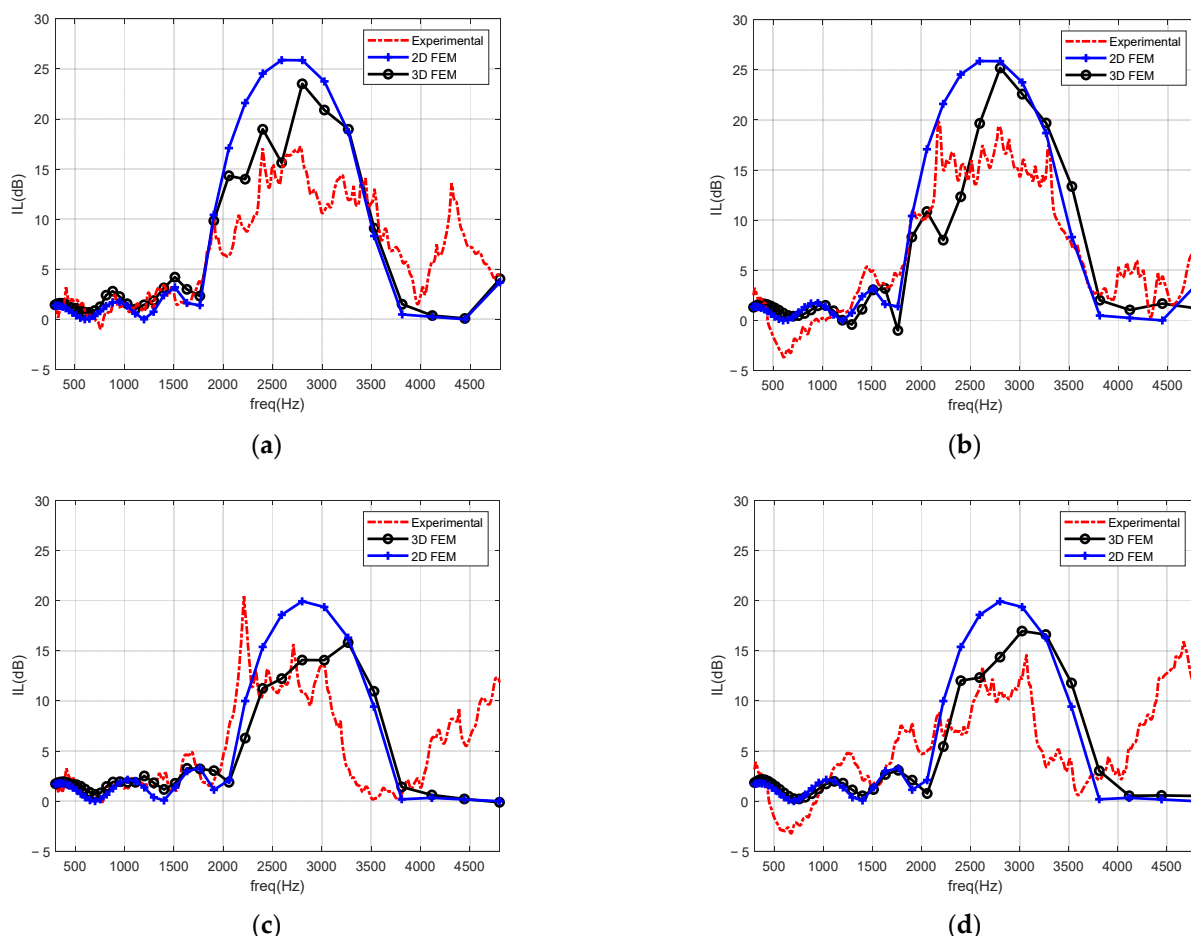
Figure 8. Measured and simulated (2D and 3D FEM model) results for reduced-scale sonic crystal barriers with different scatterer distributions: (**a**) 1.2 m tall, rectangular arrangement; (**b**) 0.6 m tall, rectangular arrangement; (**c**) 1.2 m tall, triangular arrangement; (**d**) 0.6 m tall, triangular arrangement.

The analysis of the results for the triangular arrangement of scatterers, in Figure 8c,d, reveals less clear results, particularly when the smaller barrier is analyzed. For that case, the band gap structure is less evident, and a second peak of high IL attenuation has been registered above 4500 Hz, which does not occur in the numerical FEM models' results. It should be noted that there are some differences between the experimental setup and the numerical model, one of them being related to the type of sound source used; in the experimental setup, a loudspeaker (closer to a point source) is used, while in the numerical

models a continuous load (plane wave for 2D or line load for 3D) is modeled, and this has an effect on the registered IL values. Indeed, in the case of the loudspeaker, oblique incidence angles are introduced, and this can induce some changes in the scattering pattern inside the sonic crystal. This can be seen in results presented in [28], using a smaller-scale setup, and in which the second peak is clearly visible for the triangular lattice.

4.2. Numerical Simulation Analyses

4.2.1. Effect of Number of Scatterers

Different numerical simulations have been performed in the scope of this work, in order to complement existing results and analyses found in the literature regarding sonic crystal barriers. For that purpose, the 2D FEM model was initially used, simulating both the rectangular and the triangular sonic crystal arrangements, considering a lattice constant of 0.17 m. As for the reference results, numerical FEM simulations with two, three and four rows of cylindrical circular scatterers were performed, considering scatterers with a 12 cm diameter, and the corresponding insertion loss (IL) results are depicted in Figure 9. In Figure 9a, the finite element mesh used for the calculation of the cases of noise barriers with two and five rows of cylinders is illustrated, showing the increase in mesh density around the scatterers, in order to allow improved accuracy and a better reproduction of the circular geometry. On the other hand, Figure 9b,c shows the IL obtained for the rectangular and triangular sonic crystal arrangements. Analyzing Figure 9b, it becomes clear that a classical and well-defined structure of the IL curve is visible, with two significant IL peaks occurring around specific frequencies. These correspond to the band gaps described before, and the first occurs around $f = c/2\alpha \approx 1000$ Hz. As expected, the attenuation in this band gap successively increases with the number of rows, reaching around 38 dB for the periodic structure with five rows of scatterers. Similar behavior can be seen for the triangular arrangement, as depicted in Figure 9c, although it is interesting to note that lower values of the IL are achieved. These results are in line with the classical results found in the literature, such as in [11,29], and show that a barrier with four rows of cylinders can reduce sound pressure levels by more than 10 dB, in the ranges between 600 and 1200 Hz, for a rectangular arrangement of the sonic crystal (peaking around 30 dB), and between 750 and 1200 Hz, for a triangular arrangement of the scatterers (peaking around 20 dB). Indeed, both in terms of IL values and band gap width, the rectangular arrangement of the sonic crystal elements seems to allow a more interesting performance of the system.

4.2.2. Effect of Scatterers Shape and Size

For the purpose of the present work, it was also relevant to assess the effect of changing the shape of the scatterers to a square cross-section. Indeed, both circular and square cross-sections are quite simple to produce in industrial context and they could turn to be viable alternatives in the industrial production of a wood-based sonic crystal noise barrier, without large manufacturing costs variations. In both cases, the industrial processing of the wood logs is simple to perform and does not require advanced technological means. Besides, both shapes are already available in the market for different applications.

In Figure 10, the results computed considering these two different types of scatterers, namely with circular and square cross-sections, can thus be observed. The square scatterers cross-section has dimensions of 10.6 cm × 10.6 cm, while the same dimensions defined before have been used for the circular scatterers cross-section (with 12 cm diameter); with this dimension, the scatterers of both types will have the same cross-sectional area. Both for rectangular and triangular sonic crystal arrangements, the effect of a square scatterer cross-section seems to reduce the acoustic performance of the sonic crystal noise barrier, and such decrease seems to occur due to a significant reduction of the Bragg scattering effect, since the square shape hinders the formation of the multiple reflections between scatterers. The described behavior is even more evident in the case of the triangular distribution of the sonic crystal elements, where a significant reduction from a maximum attenuation IL value of 20 dB to 12 dB is registered.

In order to have a better understanding of these effects, the dispersion curves diagram and band gap structure of the two sonic crystal configurations has been computed using a FEM analysis of a unit-cell. The conventional representation in terms of wave-vectors has been used, in which directions Γ-X m correspond, respectively, to pairs of $(k_x; k_y)$ of $(0; 0)$, $(\pi/0.17; 0)$ and $(\pi/0.17; \pi/0.17)$, k_x and k_y being the wavenumbers in the two orthogonal directions of an infinite periodic structure with a lattice constant of 0.17 m. Observing the sonic crystal band gap structure, computed for the rectangular lattice and for both scatterers cross-section shapes (Figure 11), the change in the behavior of the band gap structure is also very evident. The analysis for the cross-section square scatterers indeed exhibits no complete band gap, although quite large pseudo-gaps (occurring only in part of the propagation directions) are still observed. For the propagation directions of interest in our simulations, the relevant part of this band gap structure lies between the directions Γ and X, for which a pseudo-band gap occurs between 650 Hz and 1250 Hz, for circular cross-section scatterers, and between 600 Hz and 1100 Hz, for the square cross-section scatterers, placed in square lattice sonic crystal arrangements.
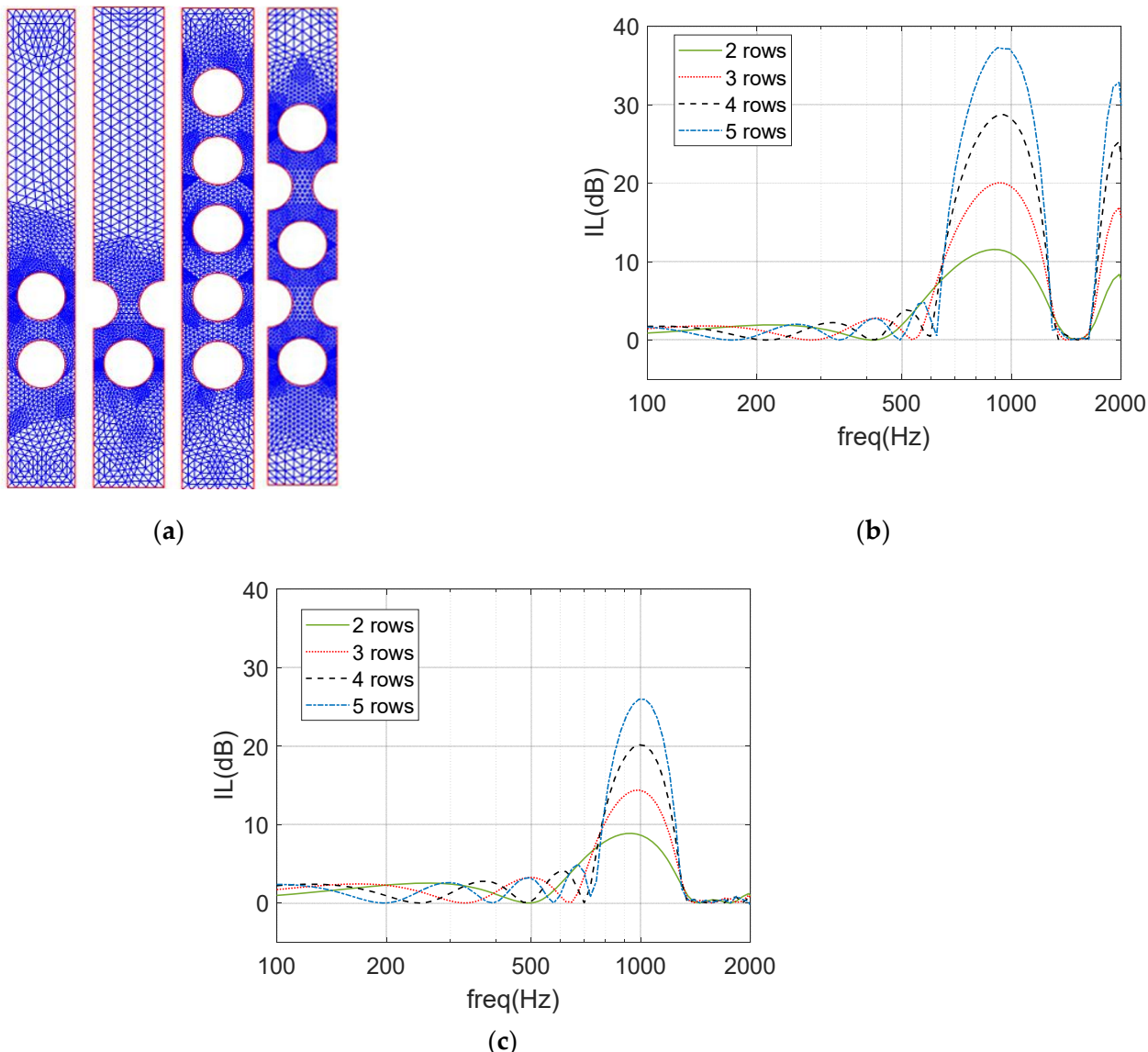
Figure 9. Reference numerical results for the regular sonic crystal barriers. (**a**) Meshes used for the cases with 2 and 5 rows of cylinders; (**b**) IL curves computed for rectangular arrangements of the scatterers; (**c**) IL curves computed for triangular arrangements of the scatterers.
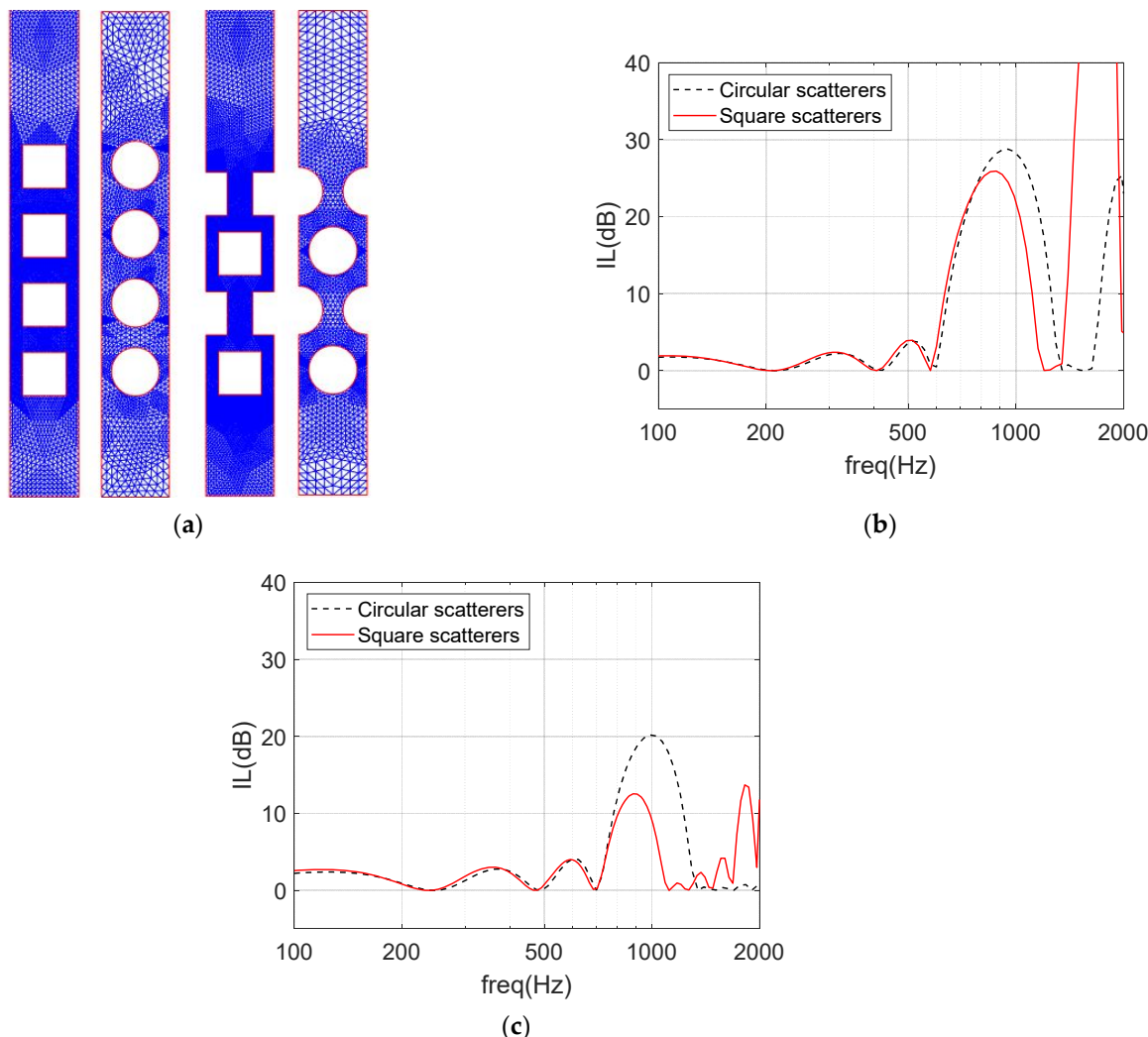
Figure 10. Effect of using square vs. circular cross-section scatterers in the sonic crystal noise barrier. (**a**) Meshes used in the numerical simulations; (**b**) IL curves computed for rectangular arrangements of the scatterers; (**c**) IL curves computed for triangular arrangements of the scatterers.
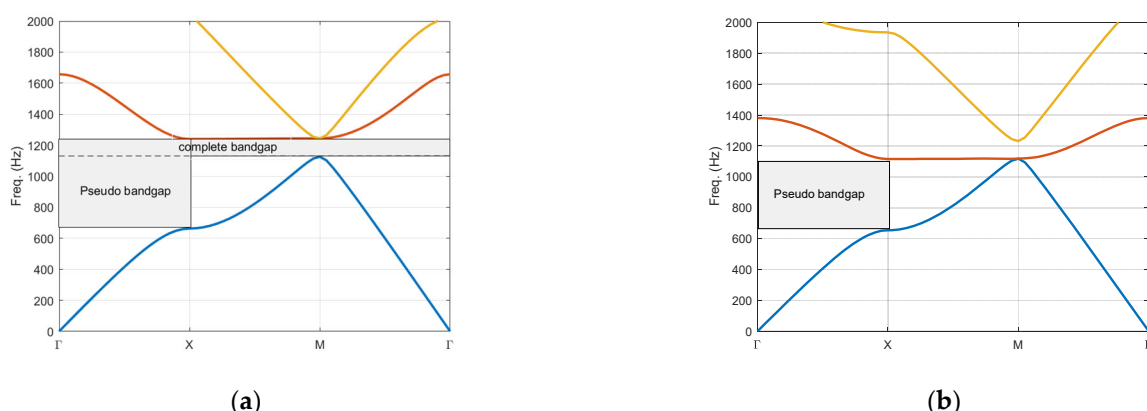
Figure 11. Dispersion curve diagrams for a square lattice sonic crystal with $\alpha = 0.17$ m and for different cross-sections: (**a**) circular, and (**b**) square scatterers.

An additional set of numerical simulations was performed, aiming to better understand the possible effect of considering a different row of scatterers, either in one of the inner rows or in the extreme rows of the sonic crystal noise barrier. For that purpose, the

sonic crystal configuration with circular scatterers with a diameter of 12 cm was analyzed, with a reduction in the scatterer diameter in one of the rows of the noise barrier to half the initial value (6 cm). This analysis was performed both for the triangular and for the rectangular arrangements of the sonic crystal scatterers. Figure 12 depicts the results obtained for the two types of arrangements, including the reference case (with all the scatterers of the sonic crystal with the same size). Observing these results, it is evident that, in all cases, the maximum value of the IL, occurring at the sonic crystal band gap, decreased by as much as 7 dB, for the rectangular arrangement of the scatterers, and by 4 dB, for the triangular spatial distribution case; the IL curves computed when the smaller scatterer was at one of the extremities of the sonic crystal seem to coincide almost perfectly, and so do the two curves computed when the smaller scatterer was in an inner row of the sonic crystal. However, it is interesting to note that, when the smaller circular element was inside the sonic crystal, a second IL peak seems to have appeared at lower frequencies, with a relevant attenuation magnitude (around 10 dB at 550 Hz, for the rectangular arrangements of the scatterers, and 600 Hz, for the triangular spatial distribution case), and also that at lower frequencies a small increase in the IL values also occurs. This effect can be important, since it may have allowed us to provide some additional (but significant) attenuation at frequencies otherwise unaffected by the presence of the sonic crystal noise barrier. To further clarify this effect, the IL curves computed in 1/3 octave bands (considering five frequencies per band) are represented in Figure 13a, for the three groups of curves, considering the rectangular arrangement of the scatterers; in addition, in Figure 13b, the normalized road traffic noise spectrum (as depicted in Figure 2) is displayed, together with the expected sound pressure level reduction provided by each of the sonic crystal noise barriers (calculated, at each frequency, by subtracting the IL values from the corresponding traffic noise spectrum values). It may be inferred that the effect, at lower frequencies, is not negligible, and may be useful in some cases to allow some additional control at lower frequencies. The global value of the A-weighted sound pressure level parameter, LA_{eq} (in dB(A)), has been computed considering just the 1/3 octave frequency bands between 100 Hz and 2000 Hz, and it is displayed also in association with each of the depicted curves, showing that, however, almost no global reduction (around 0.2 dB(A)) is provided by including a different scatterer row.


(a)

(b)

Figure 12. *Cont.*

(c)　　　　　　　　　　　　　　　　　　　　　　　(d)
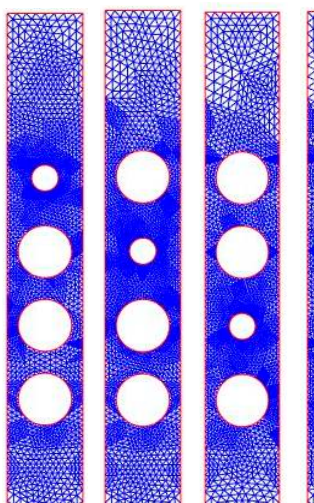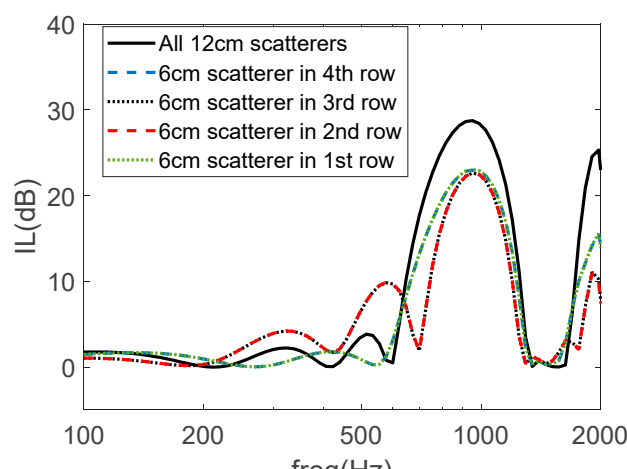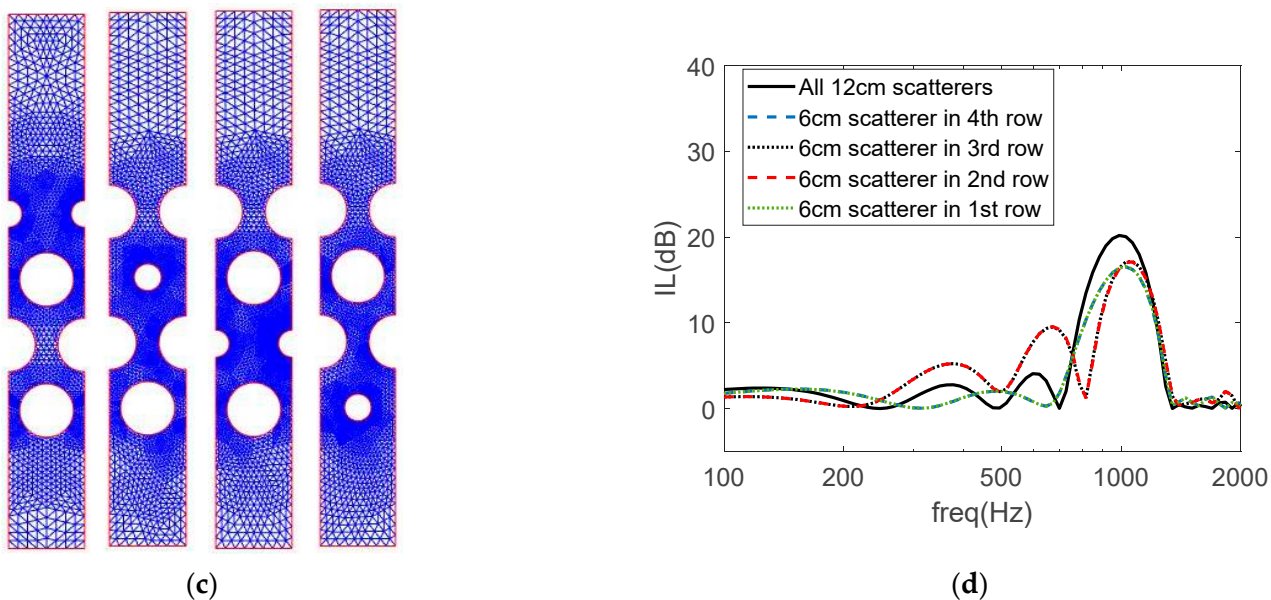
Figure 12. Effect of a different scatterer in one of the rows of the sonic crystal barrier. (**a**) Meshes used in the numerical simulations for rectangular arrangements of the scatterers; (**b**) IL curves computed for rectangular arrangements; (**c**) meshes used in the numerical simulations for triangular arrangements; (**d**) IL curves computed for triangular arrangements.

(a)　　　　　　　　　　　　　　　　　　　　　　　(b)
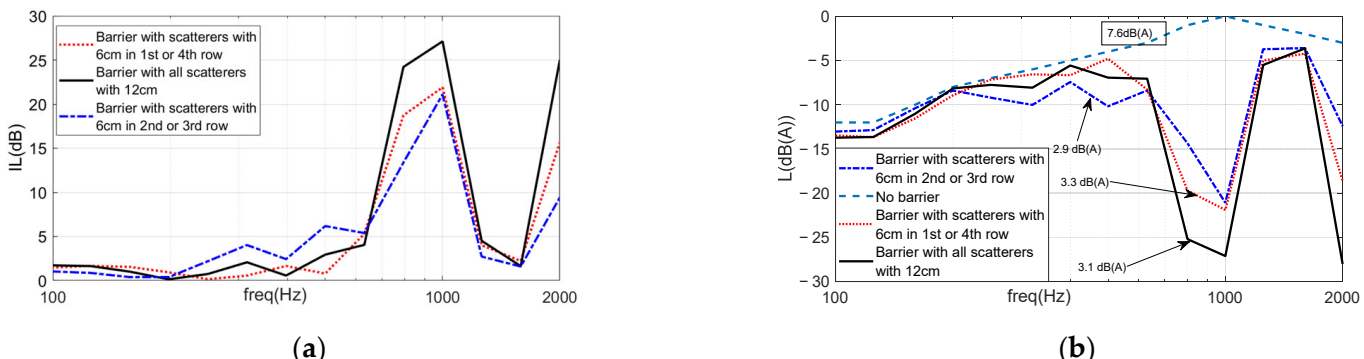
Figure 13. Effect of a different scatterer on one of the rows of the sonic crystal barrier. (**a**) 1/3 octave band IL curves; and (**b**) effect on the normalized traffic noise spectrum sound level perception, for the rectangular arrangement of the scatterers with one row with a smaller scatterer.

4.2.3. Effect of Random Variations in the Scatterers

An important effect that occurs when using natural materials, as it is the case in the present work with timber logs, is that, despite any wooden surface treatments, some random variations may occur from scatterer to scatterer, since wooden elements may vary their size non-uniformly due to temperature and moisture content, or they may even initially present some slight deviations. In addition, it is common that the implementation of a given solution in a construction site may suffer with defects and misalignments in the positioning of the different elements of the noise barrier. In this regard, Figure 14 illustrates one of the sonic crystal specimens built in the laboratory, with the wooden scatterers exhibiting large deviations from the originally designed alignment. To assess the relevance of such effects, numerical simulations have been performed considering random variations of the scatterer diameter and of the distance between rows. As a reference, the rectangular arrangement of the scatterers with four rows has been analyzed. One should notice that the position and the diameter of the scatterers is kept constant throughout each row, thus keeping the periodicity along the longitudinal direction of the barrier.

Figure 14. Example of deviations in the position of the scatterers in a wooden sonic crystal noise barrier.

Figure 15a illustrates the IL variation range achieved by the sonic crystal noise barriers when the diameter of the scatterers is allowed to vary up to 3 cm from the reference 12 cm diameter value. In total, 100 cases were run, considering that this random change occurs at each scatterer independently (in fact, because of the periodicity of the system, this occurs at each row of scatterers independently). On the other hand, Figure 15b presents a histogram showing the diameter randomness throughout the whole set of simulations. Observing the IL plot (Figure 15a), it is possible to conclude that the randomness of the scatterer diameter indeed may affect the acoustic behavior of the sonic crystal structure, up to a point of reducing the peak IL value around 10 dB when compared to that of the reference case (all scatterers 12 cm in diameter). Interestingly, outside the sonic crystal band gap the behavior is less predictable, with some IL improvements occurring for the maximum IL curve. This is in line with the behavior occurring when one different scatterer is introduced, as described before. In Figure 16, the effect of randomness in the spacing between rows of sonic crystal elements (deviations of up to 2 cm from the expected position) is shown, revealing an interesting acoustic behavior. Indeed, for this case, significant positive effects are registered, indicating that, in some cases, some randomness may even be beneficial to the acoustic attenuation performance of the noise barrier. For this case, the reference curve lies within the envelope of the randomly tested cases. Finally, Figure 17 illustrates the joint effect of both randomizations (scatterer diameter and positioning), revealing a very large envelope of possible IL values at mid and high frequencies.

(**a**)

(**b**)
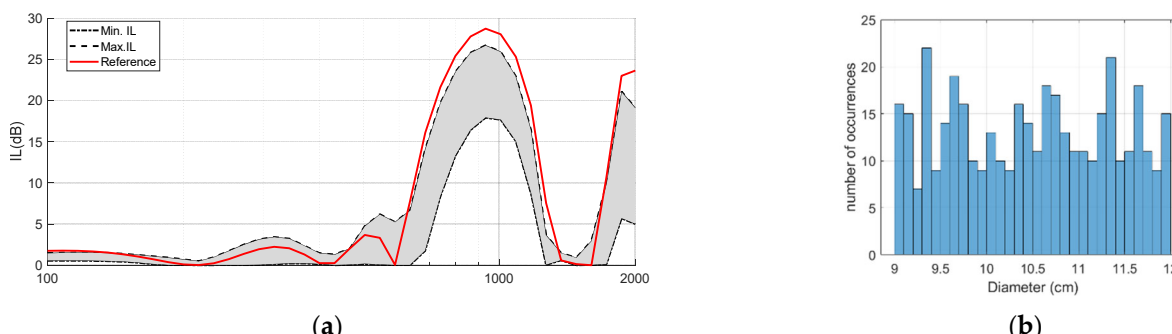
Figure 15. (**a**) IL variation range resulting from randomization of scatterer diameter (ranging from 9 to 12 cm); (**b**) histogram of the diameter variation throughout the 100 random cases.
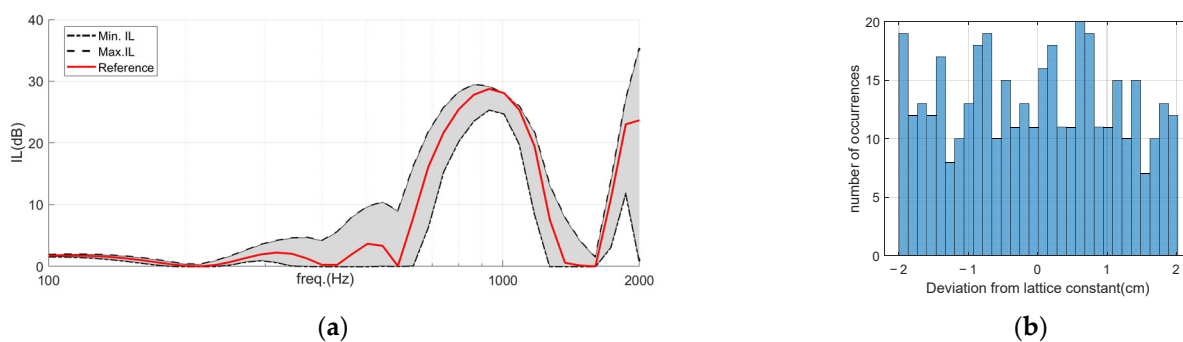
Figure 16. (**a**) IL variation range resulting from randomization of scatterer position (up to 2 cm from reference position); (**b**) histogram of the position deviation throughout the 100 random cases.
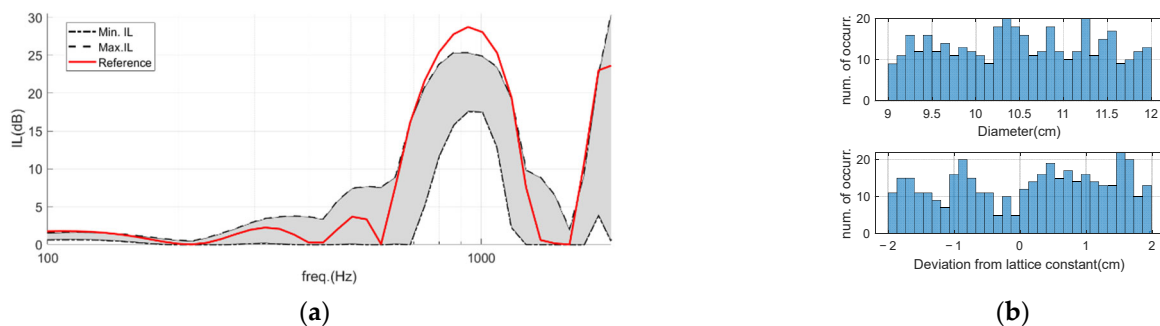
Figure 17. (**a**) IL variation range resulting from randomization of joint scatterer position and diameter; (**b**) histograms of the position deviation and diameter variation.

5. Conclusions

The present study has focused on the experimental and numerical analyses of wooden sonic crystals applied as noise barriers for road traffic noise reduction. For their implementation, sustainable elements, made up of wood logs obtained, namely, from forest thinning operations, have been used. Different geometric configurations have been built and experimentally analyzed, in order to evaluate the barriers' insertion loss acoustic performance, at the acoustic laboratory of the Department of Civil Engineering of the University of Coimbra.

An important set of numerical simulations have also been performed making use of 2D and 3D FEM approaches, in order to investigate the effect of the number of scatterers on the rows of the sonic crystal noise barriers, the effect of the scatterer cross-section shape and size, and the effect of random variations on the scatterer size and positioning. The results obtained in the laboratory tests have been compared to the results given by numerical simulations, allowing the validation of the implemented numerical models. The responses from both study approaches (numerical and experimental) have achieved very interesting levels of acoustic attenuation, in terms of the computed insertion loss values provided by the noise barriers, also revealing good agreement with the adopted evaluation methodologies. In fact, the analysis of the significant number of sonic crystal configurations, tested in the laboratory and numerically simulated, have shown that the attenuation levels provided by this type of noise barrier tends to increase with a higher number of rows of circular cross-section scatterers, arranged in square spatial distributions. One can note that maximum Insertion Loss values above 25 dB were observed at frequency bands corresponding to the greatest interaction with the sonic crystal.

Therefore, the studied sonic crystal noise barriers can be recommended as effective solutions in reducing noise generated by road traffic, while addressing some problems usually associated with conventional noise barrier solutions, such as diffraction at the edges of the barrier, the reflection of the incident acoustic waves in opaque plane barriers, and the reduced transmission of air and light through those more traditional barrier solutions.

In addition, sonic crystal noise barriers can be identified to have other advantages. In fact, with scatterers being made up of recycled byproducts or natural materials, such as wood derivatives or whole wood logs, this type of noise barrier solution is in agreement with current environmental green policies, including the sustainable development goals of the United Nations and circular economy principles. The proposed solution can therefore be seen as a technologically simple and sustainable solution, with high potential in the mitigation of road traffic noise.

References

1. Muzet, A. Environmental noise, sleep and health. *Sleep Med. Rev.* **2007**, *11*, 135–142. [CrossRef] [PubMed]
2. Babisch, W. Road traffic noise and cardiovascular risk. *Noise Health* **2008**, *10*, 27–33. [CrossRef] [PubMed]
3. Lercher, P.; Evans, G.W.; Meis, M. Ambient noise and cognitive processes among primary schoolchildren. *Environ. Behav.* **2003**, *35*, 725–735. [CrossRef]
4. Van Kempen, E.; Babisch, W. The quantitative relationship between road traffic noise and hypertension: A meta-analysis. *J. Hypertens.* **2012**, *30*, 1075–1086. [CrossRef] [PubMed]
5. De Kluizenaar, Y.; Janssen, S.A.; van Lenthe, F.J.; Miedema, H.M.; Mackenbach, J.P. Long-term road traffic noise exposure is associated with an increase in morning tiredness. *J. Acoust. Soc. Am.* **2009**, *126*, 626–633. [CrossRef] [PubMed]
6. Licitra, G.; Moro, A.; Teti, L.; Del Pizzo, A.; Bianco, F. Modelling of acoustic ageing of rubberized pavements. *Appl. Acoust.* **2019**, *146*, 237–245. [CrossRef]
7. Garai, M.; Guidorzi, P. European methodology for testing the airborne sound insulation characteristics of noise barriers in situ: Experimental verification and comparison with laboratory data. *J. Acoust. Soc. Am.* **2000**, *108*, 1054–1067. [CrossRef]
8. Asdrubali, F. On the experimental evaluation of the performances of noise barrier diffracting devices. *Acta Acust. United Acust.* **2007**, *93*, 659–669.
9. Lee, J.; Kim, J.; Park, T.; Chang, S.; Kim, I. Reduction Effects of Shaped Noise Barrier for Reflected Sound. *J. Civ. Environ. Eng.* **2015**, *5*, 1.
10. Asdrubali, F.; Pispola, G. Properties of transparent sound-absorbing panels for use in noise barriers. *J. Acoust. Soc. Am.* **2007**, *121*, 214–221. [CrossRef]
11. Gupta, A. A review on sonic crystal, its applications and numerical analysis techniques. *Acoust. Phys.* **2014**, *60*, 223–234. [CrossRef]
12. Peiró-Torres, M.D.P.; Redondo, J.; Bravo, J.M.; Pérez, J.S. Open noise barriers based on sonic crystals. Advances in noise control in transport infrastructures. *Transp. Res. Procedia* **2016**, *18*, 392–398. [CrossRef]
13. Godinho, L.; Santos, P.G.; Amado-Mendes, P.; Pereira, A.; Martins, M. Experimental and numerical analysis of sustainable sonic crystal barriers based on timber logs. In Proceedings of the EuroRegio2016, Porto, Portugal, 13–15 June 2016.
14. Rayleigh, L. XVII. On the maintenance of vibrations by forces of double frequency, and on the propagation of waves through a medium endowed with a periodic structure. *Lond. Edinb. Dublin Philos. Mag. J. Sci.* **1887**, *24*, 145–159. [CrossRef]
15. Veselago, V.G. The electrodynamics of substances with simultaneously negative values of ε and μ. *Sov. Phys. Usp.* **1968**, *10*, 509. [CrossRef]
16. Yablonovitch, E. Inhibited Spontaneous Emission in Solid-State Physics and Electronics. *Phys. Rev. Lett.* **1987**, *58*, 2059. [CrossRef] [PubMed]
17. John, S. Strong localization of photons in certain disordered dielectric superlattices. *Phys. Rev. Lett.* **1987**, *58*, 2486. [CrossRef]
18. Kittel, C. *Introduction to Solid State Physics*, 8th ed.; Wiley: New York, NY, USA, 2005.

19. Martínez-Sala, R.; Sancho, J.; Sánchez, J.V.; Gómez, V.; Llinares, J.; Meseguer, F. Sound attenuation by sculpture. *Nature* **1995**, *378*, 241. [CrossRef]

20. Sigalas, M.M.; Economou, E.N. Attenuation of multiple-scattered sound. *Europhys. Lett.* **1996**, *36*, 241. [CrossRef]

21. Fredianelli, L.; Del Pizzo, A.; Licitra, G. Recent Developments in Sonic Crystals as Barriers for Road Traffic Noise Mitigation. *Environments* **2019**, *6*, 14. [CrossRef]

22. Hirsekorn, M.; Delsanto, P.P.; Batra, N.K.; Matic, P. Modelling and simulation of acoustic wave propagation in locally resonant sonic materials. *Ultrasonics* **2004**, *42*, 231–235. [CrossRef]

23. Morandi, F.; Marzani, A.; De Cesaris, S.; Barbaresi, L.; Garai, M. Sonic crystals as tunable noise barriers. *Riv. Ital. Acust.* **2017**, *40*, 1–19.

24. Iannace, G.; Ciaburro, G.; Trematerra, A. Metamaterials acoustic barrier. *Appl. Acoust.* **2021**, *181*, 108172. [CrossRef]

25. *ISO 717-1*; Acoustics—Rating of Sound Insulation in Buildings and of Building Elements—Part 1: Airborne Sound Insulation. ISO, International Organization for Standardization: Geneve, Switzerland, 2013.

26. *EN 1793-3*; Road Traffic Noise Reducing Devices—Test Method for Determining the Acoustic Performance—Part 3: Normalized Traffic Noise Spectrum. CEN, European Standard: Brussels, Belgium, 1997.

27. Santos, P.; Carbajo, J.; Rui, D.; Godinho, L.; Mendes, P.A.; Soriano, J.R. Insertion loss provided by sonic crystal type barrier— Experimental and numerical evaluation on a reduced scale model. In Proceedings of the 45° Congreso Espanol de Acustica, Murcia, Spain, 29–31 October 2014.

28. Amado-Mendes, P.; Godinho, L.; Santos, P.G.; Dias, A.G.; Martins, M. Laboratory and full-scale experimental evaluation of the acoustic behaviour of sonic crystal noise barriers. In Proceedings of the International Congress on Acoustics, Buenos Aires, Argentina, 5–9 September 2016.

29. Morandi, F.; Miniaci, M.; Marzani, A.; Barbaresi, L.; Garai, M. Standardised acoustic characterisation of sonic crystals noise barriers: Sound insulation and reflection properties. *Appl. Acoust.* **2016**, *114*, 294–306. [CrossRef]

30. Pichard, H.; Richoux, O.; Groby, J.P. Experimental demonstrations in audible frequency range of band gap tunability and negative refraction in two-dimensional sonic crystal. *J. Acoust. Soc. Am.* **2012**, *132*, 2816–2822. [CrossRef]

31. Cavalieri, T.; Cebrecos, A.; Groby, J.P.; Chaufour, C.; Romero-García, V. Three-dimensional multiresonant lossy sonic crystal for broadband acoustic attenuation: Application to train noise reduction. *Appl. Acoust.* **2019**, *146*, 1–8. [CrossRef]

32. Rubio, C.; Castiñeira-Ibáñez, S.; Uris, A.; Belmar, F.; Candelas, P. Numerical simulation and laboratory measurements on an open tunable acoustic barrier. *Appl. Acoust.* **2018**, *141*, 144–150. [CrossRef]

33. Alagoz, S. A sonic crystal diode implementation with a triangular scatterer matrix. *Appl. Acoust.* **2014**, *76*, 402–406. [CrossRef]

34. Koussa, F.; Defrance, J.; Jean, P.; Blanc-Benon, P. Acoustical efficiency of a sonic crystal assisted noise barrier. *Acta Acust. United Acust.* **2013**, *99*, 399–409. [CrossRef]

35. Koussa, F.; Defrance, J.; Jean, P.; Blanc-Benon, P. Transport noise reduction by low height sonic crystal noise barriers. In Proceedings of the Société Française d'Acoustique, Nantes, France, 23 April 2012.

36. Lee, H.M.; Lim, K.M.; Lee, H.P. A maze structure for sound attenuation. *Appl. Acoust.* **2017**, *115*, 88–92. [CrossRef]

37. Gulia, P.; Gupta, A. Traffic Noise Control by Periodically Arranged Trees. In Proceedings of the International Conference on Recent Trends and Developments in Environmental Sustainability RTDES 2016, Chandigarh, India, 16 May 2016.

38. Martínez-Sala, R.; Rubio, C.; García-Raffi, L.M.; Sánchez-Pérez, J.V.; Sánchez-Pérez, E.A.; Llinares, J. Control of noise by trees arranged like sonic crystals. *J. Sound Vib.* **2006**, *291*, 100–106. [CrossRef]

39. Godinho, L.; Redondo, J.; Amado-Mendes, P. The method of fundamental solutions for the analysis of infinite 3D sonic crystals. *Eng. Anal. Bound. Elem.* **2019**, *98*, 172–183. [CrossRef]

40. Jean, P.; Defrance, J. Sound propagation in rows of cylinders of infinite extent: Application to sonic crystals and thickets along roads. *Acta Acust. United Acust.* **2015**, *101*, 474–483. [CrossRef]

41. Morgado, T.; Rodrigues, J.; Machado, J.S.; Dias, A.M.P.G.; Cruz, H. Bending and Compression strength of Portuguese Maritime pine small-diameter poles. *For. Prod. J.* **2009**, *59*, 23–28.

42. Atalla, N.; Sgard, F. *Finite Element and Boundary Methods in Structural Acoustics and Vibration*, 1st ed.; CRC Press: Boca Raton, FL, USA, 2015.